UNCONVENTIONAL RESOURCES TECHNOLOGY CONFERENCE
FUELED BY SPE • AAPG • SEG

URTeC: 2697437

Integration of Large-Area SEM Imaging and Automated Mineralogy-Petrography Data for Justified Decision on Nano-Scale Pore-Space Characterization Sites, as a Part of Multiscale Digital Rock Modeling Workflow

Andrey Kazak*, Svyatoslav Chugunov, Victor Nachev, Mikhail Spasennykh (Center for Hydrocarbon Recovery, Skolkovo Institute of Science and Technology);
Anatolii Chashkov (NOVATEK);
Eugenij Pichkur, Mikhail Presniakov, Alexander Vasiliev (National Research Center «Kurchatov Institute»)

Summary

Reliable characterization of complex reservoirs is tightly coupled to studying their microstructure at a variety of scales and requires departure from traditional petrophysical approaches and deepening into the world of nano-scale. A promising method of retaining representatively large volume of a rock sample while achieving nanoscale resolution is based on multiscale digital rock technology. The smallest scale of this approach is often realized in the form of several 3D FIB-SEM models, registration of these models to larger volume of rock sample, as well as estimation and upscaling of models' local properties to the volume of the entire sample. However, justified and automated selection of representative regions for building FIB-SEM models poses a big challenge to a researcher. In this work, our objective was to integrate advanced multiscale SEM technology and modern mineral mapping technology, to make a justified decision on location of representative zones for FIB-SEM analysis of a rock sample. The procedure is based on two experimental methods. The first method is an automated quantitive mineralogy and petrography scanning method that allows covering sample's cross-section with a mineralogy map, having resolution down to 1 μm/pixel. The second method targets automated mapping of sample's surface area with the use of backscattered electrons and secondary electrons; this method has resolution down to nanometers and spatial coverage up to centimeters (large-area high-resolution SEM imaging). Data gathered with both methods on millimeter-sized cross-sections of rock samples were registered and integrated in the paradigm of joint data interpretation, augmented with image processing techniques, to provide a reliable classification of nanoscale and microscale features on samples' cross-section. The superimposed SEM and mineral map images were combined with physics-based selection criteria for reasonable selection of FIB-SEM candidates out of a great number of potential sites. In the result, an automated workflow was built. Demonstration of the workflow is made on one of Russian most promissing tight gas formation, where pore space includes objects ranging from single nanometers up to millimeters. An example of optimal site selection for FIB-SEM operations, as well as an example of a typical FIB-SEM model are discussed. Basic correlation to petrophysical properties of rock is performed.

Introduction

It is commonly accepted by professionals in geoscience community, including petroleum industry, that rock physical-chemical properties and its response to static and dynamic impact in the process of technological stimulation are strongly dependent on a combination of its fabric and composition (Goergen·et·al.·2014). Studying rock texture in combination with mineralogy characterization of hard-to-recover reservoirs is significant to understand rock mechanical behavior during rock fracturing stimulation (Hussain·et·al.·2016, p. 9, Plumb, Herron,·and·Olsen·1992, Plumb·1994). Technological stimulation of reservoir rock is an operation spanning over variety of scales, starting from the near-wellbore zone (10s÷100s of meters) and finishing at pore-scale (nanometers, for tight gas formations).

Exploration, appraisal, and development phases of tight gas projects require integration of multiple scales of study (from basin to nanopores) and application of advanced tools, including scanning electron microscopy (SEM) and automated mineralogical mapping (Mathieu·et·al.·2016).

Microscale and nanoscale features significantly contribute to rock behavior during stimulation and development stages, at the same time, not many laboratory methods are available for reliable characterization of small scale processes in rock. Petrophysical techniques are mostly applicable in the range of millimeters to centimeters, while mechanical, thermal, and chemical stimulation processes take place at microsized grains, pores, fractures, and nanopores. Addressing individual characteristics of micro- and nano-features in rock helps to properly account for intrinsic details of physical interactions and to significantly improve quality of stimulation work.

The presented study is focused on application of multi-scale characterization approach to one of Russian most promising tight gas formation located in West Siberia of Russian Federation (Figure 1). The formation belongs to Supra-Cenomanian deposits of the Lower-Berezov subsuite (Berezov formation), attributed to Lower Cretaceous geological period (K_{2cn}–K_{2kp}, 88.5÷65 Ma). Hydrocarbon accumulations of Berezov formation are associated with siliceous remains of radiolarians, shells or frustules of diatoms, spicules of sponges, etc., dwelled at shallow sea areas. The reservoir rock is mostly represented by dark-grey gaze(opoka)-like clays, siliceous mudstones with rare interbeds of argillaceous siltstones and fine-grained sandstones. Exploration maturity of the Supra-Cenomanian deposits in West Siberian region is extremely low, as most wells are drilled for deeper geological intervals, passing Berezov formation with minimal information collected. Presence of hydrocarbons in deposits of Berezov formation was detected by numerous gas seeps while drilling wells at vast territory of West Siberia (Agalakov·and·Bakuev·1992). Methane gas fraction measured while drilling in the depth interval of Berezov formation varies in a range of 97÷99% (Bondarev·et·al.·2008a, b) and associated with argillaceous gazes (opoka) with high porosity of 15÷20% and pore size spanning from nanometers to hundreds of micrometers. Considering relatively low depth (900÷950 m TVDSS) and the presence of a large (1000s of wells) stack of transit producing wells, gas deposits of Berezov formation are considered a development target to be recompleted after production of gas from underlying deposits is finished. Economic feasibility of exploration and development of Lower-Berezov deposits is additionally underlined by the absence of significant expenditures for surface infrastructure development.

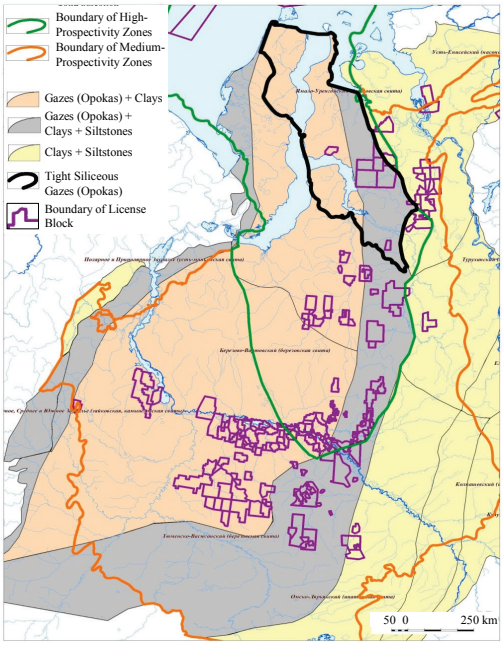

Figure 1: Map of lithological species and prospectivity of Berezov fomration on the territory of West Siberia, Russian Federation [modified after (Borodina·2016)].

Preliminary tests of gas recovery from Berezov formation, independently performed by a few gas-producing companies, were not successful — the promising gas seeps observed at drilling stage did not match the low flow figures during production attempts. The root cause for low productivity of the tested interval can be related to complex physical properties of formation rock. Substantial hydrophilicity of gaizes lead to formation of extensive zones around the wellbore, invaded with water-based drilling mud. Porosity and permeability in such zones demonstrate dramatic degradation due to clay and gaize swelling. Despite the indications of substantial gas content of Berezov formation (Bondarev·et·al.·2008b), its production potential has not been fully unveiled.

After thorough estimation of positive and negative aspects of traditional rock characterization techniques applied to rock samples of Berezov formation, it was decided to intervene into multi-scale study of rock, in order to restore 3D rock structure at macro, micro, and nano-scale, as well as to gain low-level access to specific details of physical processes responsible for rock fracturing and fluid filtering, via numerical simulations and laboratory experiments.

The further investigations of lower Berezov subsuite should include sweet spot localization, optimization of drilling-in and well completion technologies. It is also required to develop special methods for drilling through the target intervals with non filterable and waterless muds. In the optimal case, wells should be completed either through a single production string or in open hole through slotted filter liner. The expected results of the study include:

- understanding pore-scale reservoir model and pore network behavior during rock fracturing and fluid filtering;
- realistic ranges of inputs parameters for accurate estimation of gas resource, consolidated in Berezov formation;
- list of requirements for selecting the optimal technology of gas field development.

Methods and results presented in this work constitute a part of the joint Skoltech & NOVATEK project on multi-scale rock characterization, developed in the scope of joined R&D activity. In the project, there was raised a question of selecting representative zones in micro-scale rock samples for further investigation of these zones at nano-scale via FIB-SEM and EDS techniques. The data acquired at micro-scale with the help of Computed Tomography and laboratory petrophysical evaluations had too low resolution to be suitable for selecting the representative zones. A combination of automated mineralogy and large-area high-resolution SEM (a large 2D map produced by stitching hundreds of SEM images) technology proved to be useful at this task, since these methods provide spatially-resolved information on rock mineralogy, texture, grain interfaces, and other local rock parameters at fine scale. Resolution of these methods allowed successful analysis of submicron features and components of rock.

Both, automated mineralogy and large-area high-resolution SEM technologies are essentially 2D mapping techniques of a flat sample surface; they utilize a scanning electron microscope with a set of hardware attachments to collect the initial data. Automated mineralogy technology is based on generating 2D mineral maps of rock surface, using a combination of energy-dispersive X-ray spectroscopy, secondary emission (SE) electron images, and a special software system for mineral classification (Sølling, Mogensen, and Gerwig 2014). In the presented work, a proprietary software system produced by FEI company was used for mineral classification with resolution around 1 μm/pixel. Large-area high-resolution SEM technology is based on stitching a set of regular SEM images, acquired in back-scattered (CBS) or secondary emission (SE) mode, into a large mosaic map, covering the entire area of interest; the resolution of the method is determined by resolution of individual SEM images — it may reach down to 2 nm/pixel with modern SEM devices. Both methods allow quantitative appraisal of rock samples with characteristic dimensions up to 30÷50 mm, which corresponds to spatial dynamic range (sample size to pixel size ratio) of 5×10^4 for automated mineralogy and 50×10^7 for large-area high-resolution SEM. Spatially registered datasets acquired with both techniques allow propagating quantitive information on mineral composition and fabric of rock between micro- and nano-scale.

Integrating automated mineralogy and SEM (mostly CBS images) techniques was recently proposed by a few research groups (Schembre-McCabe, Salazar-Tio, and Kamath 2012, Lattanzi et al. 2014, Madi and Belhadj 2015). Image processing of SEM images and mineral maps provides input data for computing the so-called Rock Texture Index, using an equation that combines rock mineralogy and texture, excluding total organic content and cracks (Hussain et al. 2017). An accurate prediction of crack length as a function of grain size and porosity could be established via analysis of rock texture and crack tortuosity (Minhas et al. 2016), using SEM images. The introduction of large-area high-resolution SEM technology instead of a regular SEM pushed the limits of such integrated analysis even further (Liao et al. 2015). Some examples of successful application of these techniques include studying of nanopores in organic matter (Fogden et al. 2015) and capturing mudrock heterogeneity via a detailed microstructural and mineralogical analysis (Goergen et al. 2014). However, there was no consistent approach applied to selecting representative sites in micro-scale rock sub-plugs for multi-scale evaluation.

The largest technically accessible sample sub-volume prepared with FIB-SEM method does not cover the entire area of interest — many grains, grain-matrix and void-matrix interfaces have the size superior to that of the studied sub-volume. Therefore, selecting proper spots for study with FIB-SEM method requires careful analysis of both, automated mineralogy and large-area high-resolution SEM data. In overwhelming majority of cases selection of FIB-SEM sites is being done in by-eye manner by image analyst working with the dual-beam microscope system and, rarely, by a professional geologist/petrologist/lithologist. Such selection is prone to human subjectiveness; it does not properly account for intrinsic characteristics of the investigated sample. Hence, development of an automated method for FIB-SEM sites selection is highly on demand.

Materials and Methods

A collection of whole core (Ø100×100 mm) pieces, taken from a single exploratory well at an interval of lower Berezov gas reservoir, was investigated with multiscale digital rock approach. The whole core pieces were isolated from the surrounding with wrapping them into a plastic film and covering with multiple wax layers, within a short

period of time after taking them from the well. Based on well log information, a few whole core pieces were selected for routine laboratory analysis and for building multi-scale digital rock models.

From the lithological standpoint, the rock samples fell mainly into two lithological categories: gaize (opoka) and tripoli (Figure 2). From petrophysical perspective, the samples had porosity 18÷26% with average value 22% and gas permeability 0.2÷60 mD with average value 11 mD. High porosity and relatively low permeability were originally associated with the presence of a large number of micro-scale voids having interconnecting nano-channels.

The whole core pieces were split into several representative standard plugs Ø30×30÷90 mm, which in turn, after analysis at macro-scale, were split into representative micro-scale mini-plugs (sub-plugs) Ø3×10 mm (Figure 3). The micro-scale sub-plugs were evaluated with a range of micro-scale analysis methods. The complete suite of laboratory methods applied to the rock samples and typical parameters used for sample imaging are shown in Table 1.

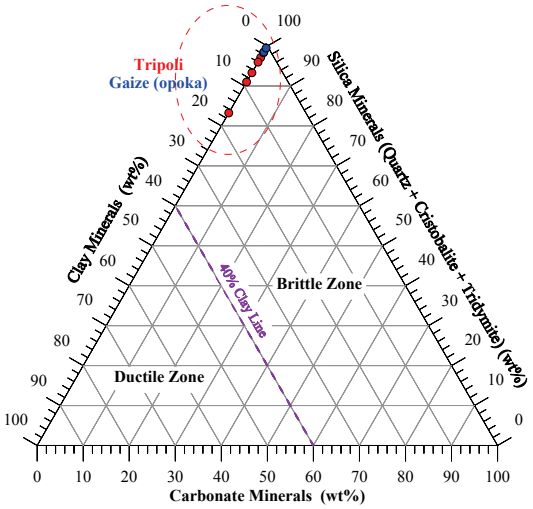

Figure 2: Mineral composition of studied rock samples.

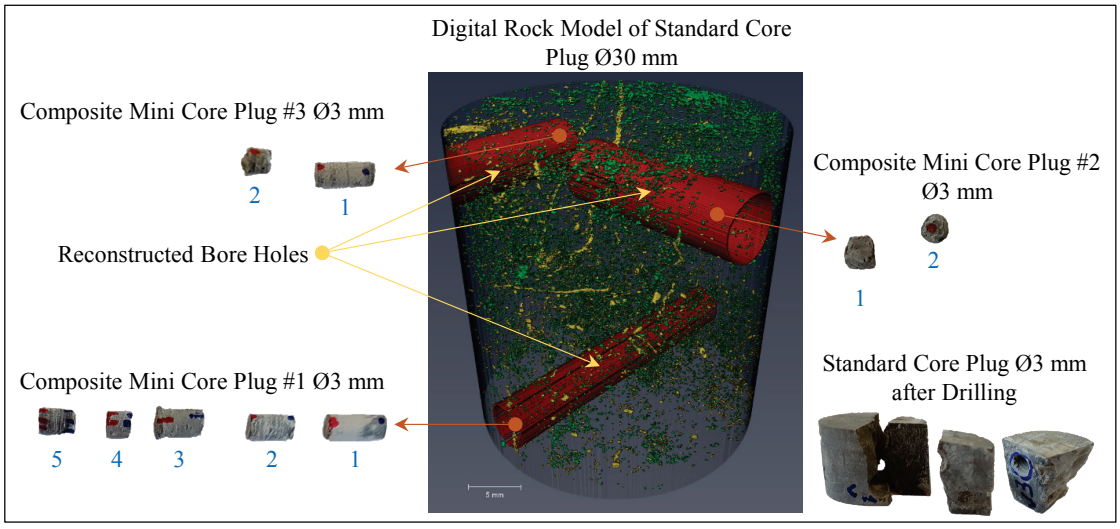

Figure 3: Illustration of separration of a standard core plug Ø30 mm into composite mini core plugs, all of which, in turn, are separated naturaly to mini core plugs Ø3 mm.

Table 1: Overview of methods used to generate multiscale 3D digital rock models.

Typical Rock Sample	Scale	Method(s)	Pixel/Voxel Size
Whole core	Macro	Photo and video capturing	10÷0.5 mm/px
Standard core plug Ø30 mm	Meso	X-ray micro CT Automated mineralogy Optical Microscopy of Thin Sections SEM in SEI and EDS single-point modes	12.5569 µm/vx 14.652 µm/px 4 µm/px 0.17÷ 1.18 nm/px
Mini core plug Ø3 mm	Micro	X-ray micro CT Automated mineralogy Large-area high-resolution SEM in CBS and ETD SE modes	970.587 nm/vx 976.801 nm/px 16.927÷134.9284 nm/px
	Nano	FIB-SEM with EDS	(XY) 4÷6 nm/px; (Z) 25 nm/px

Processing of results consisted of data quality inspection, spatial registration of SEM images to automated mineralogy data, post-processing of registered results, using MATLAB and ImageJ software. Post-processing steps included handling Unclassified and uncertain pixels in mineral maps, segmenting mineral phases and pseudo-phases, selecting corresponding zones in SEM data, analysis of texture parameters of selected features in SEM images.

Rock Sample Preparation

For the purpose of microstructural investigations using techniques such as automated mineralogy and petrography and large-area high-resolution SEM, a set of selected micro-scale core sub-plugs were cut into halves along the primary cylinder axis with a 91 µm thick diamond saw (Figure 4). One half of each pair was left in reserve, the counterpart (working half) was considered a primary sample for preparing micro-scale sub-volumes for characterization at nano-scale. Prior to application of FIB-SEM, selection of representative spots was performed.

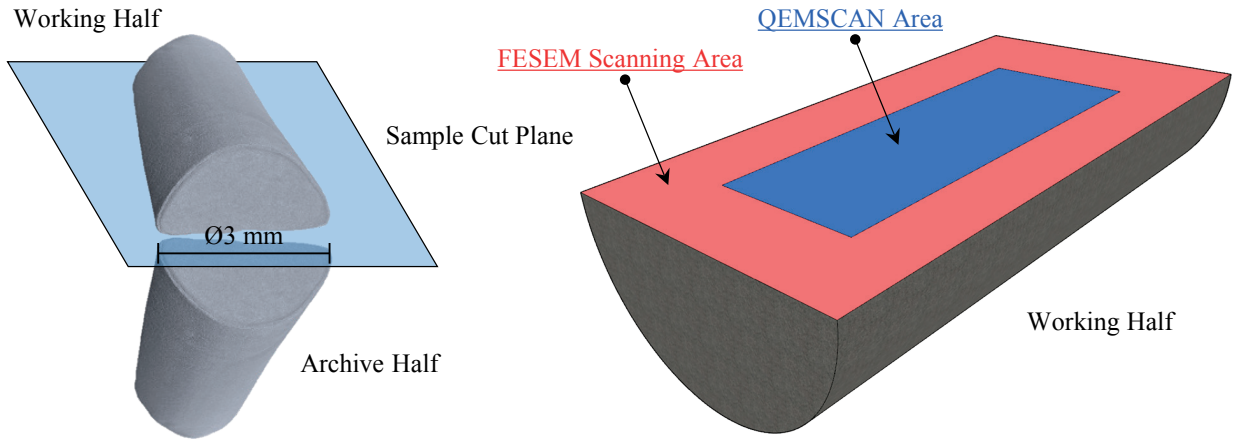

Figure 4: Schematic diagram of sample preparation and areas of investigation.

The primary half-plug was molded into Ø30 mm epoxy cylinder with the rock cut surface aligned and exposed on the cylinder's top surface, the top of the cylinder was polished and sputter-coated with a uniform 50 nm carbon film to prevent sample charging, as per requirements of the utilized automated mineralogy scanner

Acquisition of Automated Mineralogy Data

The mineral mapping of the surface was performed using specialized system FEI QEMSCAN WellSite® — an FEI scanning electron microscope (SEM) with Bruker XFlash X-ray detector for EDS analysis. Measured at a point on the sample surface, the collected X-ray spectrum enables determination of a concentration of various chemical elements at the scanned point (Goldstein·et·al.·2003). EDS analysis does not determine mineral content directly. The combination of elements at a particular location must be analyzed in order to infer the type of a mineral occupying the location. These determinations are almost always non-unique. In the presented work, conversion of elemental composition to mineral composition is done using a sophisticated algorithm (Butcher·et·al.·2000) implemented in the QEMSCAN® proprietary software. During measurements, the area to be analyzed is irradiated with a finely focused high-energy electron beam in a SEM device, the beam is swept in a raster scan pattern to form a 2D image (Goldstein·et·al.·2003). The resulting image, processed with Species Identification Protocol (SIP) enabled software, is a false-colored image, where each color corresponds to a certain mineral phase, void, background, or the Unclassified category; calibration of the system is made using pure mineral standards (Sølling, Mogensen,·and·Gerwig·2014). Typically, QEMSCAN provides a high quality of mineral classification, but, for some cases, it was reported that the technology cannot distinguish between certain minerals, for example, illite and muscovite (Bouw·and·Lutgert·2012).

Operating parameters of the SEM device applied to the rock samples of Berezov formation are shown in Table 2. The operation mode parameters were tuned up with consideration of the best possible raw data quality, in terms of signal-to-noise ratio and number of counts per unit of time on EDS detector.

Table 2: Operating parameters of FEI QEMSCAN WellSite device set for scanning target samples.

Parameter	Value
Electron Beam Accelerating Voltage	15 kV
Emission Current	48 µA
Detector Type(s)	BSE, XFlash
Operating Magnification Range	100–1500×
Analysis Type(s)	FieldImage
Distance between EDS-Spectra Acquisition Points	1 µm
EDS-Detector Count Rate	~360,000 pulse/sec
Required Level of EDS-Signal	2000 pulses
Area of Investigation	≥ 4 mm²

The lower limit of QEMSCAN resolution is about 1 µm, but often, particularly in clays, the crystallites are significantly smaller. This gives rise to the registration of more than one spectrum in a single pixel and leads to accumulation of a spectral pattern that cannot be easily reconciled with a single mineral. The result is a pixel that will be labelled as Unclassified. This can be alleviated to a certain extent by software processing but is eventually intrinsic to the sample.

Acquisition of Large-Area High-Resolution SEM Data

Table 3: Typical parameters of SEM images.

Parameter	Value
Typical Image Dimensions	30,000 × 100,000 px
Image Pixel Size	135 nm/px

Acquisition of large-area high-resolution SEM data was done with FEI Versa 3D DualBeam instrument, using CBS and ETD SE detectors (Table 3). Because data acquisition for both detectors was done simultaneously, CBS and SE images were automatically pre-registered by MAPS software. Typically, the CBS image contains better pronounced details of material heterogeneity in terms of the response of different mineral phases, while the SE image provides greater insight on mineral surface topography and efficiently highlights sharp irregularities, such as fractures between aggregates and intra-grain ruptures.

Image Registration Workflow

Prior to the integrated quantitative analysis, images produced with automated mineralogy and SEM methods were pre-processed and spatially registered. Mineral map image had an 8-bit indexed format, where each pixel had a size of 977 nm and an associated mineral index. All indices, corresponding to mineral phases, were presented in the form of a look-up table (LUT) embedded into the image. Original SEM images had pixel size 135 nm for both, CBS and SE images. The registration procedure requires rotation a translation of the source image — when rotated, data at each pixel is resampled via interpolation between neighboring pixels. If such process is applied to the mineral map image, index values would be distorted; this breaks down the integrity of the mineral map (for example, arithmetic average operation over quartz and pyrite is undefined). Therefore, mineral map image was kept intact, while SEM images were resampled and rotated/translated for spatial registration. In order to achieve high-quality results, the following image registration steps were applied to the datasets.

1) Perform image denoising and background removal procedures.
2) Downsample the original SEM image to the resolution of the mineral map image.
3) Extract landmarks (markers, control points) from the source and the target images using scale invariant feature transform (SIFT) algorithm. After features had been extracted from both, the source and the target images, they were matched to each other, in order to obtain comprehensive correlations, serving as a basis for image registration.
4) Assign the mineral map as a fixed target image and the SEM-based large-area map as a movable source image.
5) Perform image registration with several registration methods, using the set of landmarks obtained in step 4):
    a. *Translation* image transform,

   b. *Rigid* (translation + rotation) image transform,
   c. *Similarity* (translation + rotation + isotropic scaling) image transform,
   d. *Affine* (free affine transform) image transform,
   e. *Elastic* (deformations represented by B-splines or other non-linear functions) image transform.
6) Check image registration quality of each method. Adjust control parameters to achieve the best result in each case.
7) Save the optimal image registration/transformation parameters obtained for downsampled images, in order to use them for registration of images at the original SEM resolution.
8) Upsample the original mineral map to the resolution of the original SEM images for image registration at high resolution.
9) Use image registration/transformation parameters obtained in step 7) to register original SEM images to the upsampled mineral map image.
10) Check registration quality, if the results failed the quality requirements alter registration parameters or change registration method and repeat step 9), until reasonable match is achieved.

It needs to be mentioned that the main image registration mode was the *Mono* mode in ImageJ, which assumes unidirectional registration of the images (SEM images are registered to the fixed mineral map image). Other registration modes, such as *Accurate* and *Fast*, may allow the use of both images as the source and the target of registration.

Post-Processing of Automated Mineralogy Data

Original mineral map images contain information on mineral phases in terms of pure minerals, such as “Quartz”, “Albite”, “Pyrite”, and others, as well as on mixed mineral phases, such as “Quartz-Pyrite (75:25)”, “KFeldspar-Calcite (75:25)”, “Albite-Chlorite (75:25)”, and others. The latter category contains, according to QEMSCAN mineral classification scheme, two minerals within the same pixel, in proportion close to 75:25. In the real rock, many of such uncertain pixels occur in the bulk of a mineral phase, where possibility of having the second submicron mineral inclusion is quite low. For such uncertain pixels, the mineral index was replaced to the one, representing the “75” part.

Besides the pixels containing information on mineral phases, there exist *unclassified* pixels. For these pixels, the identification and classification algorithm could not reliably determine an associated mineral. This happens due to the collected X-Ray spectra being not presented in the SIP database, containing excessive noise, being well below or above the threshold values, applied by the automated mineralogy technique. Many unclassified pixels, similar to the case of uncertain pixels, occur in the middle of existing mineral phases, or surrounded by background or a pore. A moving window of a certain size was used to estimate possible values of unclassified pixels. A small rectangular neighborhood was considered for an unclassified pixel, which was at the center of the window. The most frequent element in the neighborhood was determined and assigned to the central pixel. This approach well handles the cases when single unclassified pixels are surrounded by minerals forming a majority in the neighborhood. For the cases, when a cluster of unclassified pixels is considered, pixels in the center of the cluster are surrounded with unclassified pixels, which constitute the most frequent pixel value in the neighborhood. In such cases, an iterative approach was applied, where unclassified pixels at the boundary of the cluster were replaced first, unclassified pixels next to the boundary were replaced on the next iteration and so on. The process repeats until no unclassified pixels remain in the image.

The mineral maps often contain regions where multi-mineral associations (mineral groups) are observed (Figure 5). Multi-mineral associations typically depend on diagenetic and morphological relationship between minerals — a mineral pseudo-phase could be defined for such regions. It allows replacing a group of closely spaced minerals with a single index of a pseudo-phase. For identification of pseudo-phases, a list of rules was created where minerals, forming pseudo-phases were specified. The rules were formulated in terms of binary relations — if two minerals are located at certain (small) distance from each other, they can be considered as a part of a pseudo-phase and replaced with the corresponding index value. A moving window of a certain size was used to scan mineral map image to identify all cases where minerals come close to each other. The size of the window determines the maximal distance between the minerals. If two minerals, forming a rule for a pseudo-phase, are present in the window, the flood fill process starts from each of these pixels filling all connected pixels of the same index with the index value of the resulting pseudo-phase. The algorithm was iteratively applied to the image due to the two reasons: (1) MATLAB was used for data processing, this software has a limitation for the maximum number of recursion operations, which are required for the flood fill algorithm — complete filling of large mineral phases may require a few iterative attempts; (2) at the first pass, some rules, such as “a mineral located close to the pseudo-phase is painted to that pseudo-phase”,

do not work as the logical condition is not satisfied yet, after a few passes, some minerals transform into pseudo-phases and additional rules start working. The result of this processing is the reduction of the number of mineral phases present in the image, as well as substitution of some mineral clusters with pseudo-phases.

Rock Fabric and Composition Integration Workflow

The rock fabric (also referred to as *petrofabrics* or *petrotexture*) is a system of spatial and geometric relations between all components of the studied rock. The term "fabric", coined by Sander·(1930), corresponds to rock structure, texture, predominant orientation of its components and is used to characterize shape and features of all separate rock components, their mutual arrangement and orientation in space. Rock composition is being determined by the kind and quantity of components forming the rock. Composition can be mineral or elemental, volumetric or mass, bulk or surface.

Information on rock fabric can be extracted from SEM data, but the analysis results, to be uniquely associated with a specific mineral phase or a pseudo-phase, have to be computed only over an area occupied by the analyzed component of rock. Binary masks were prepared for each analyzed component, using spatial distribution of mineral phases and pseudo-phases in mineral map images. The masks were processed with morphological closing operator to remove single-pixel artifacts that appear in the image due to the uncertainties in automated mineralogy data. Since image registration of mineral maps and large-area SEM images could not be done with subpixel precision, small deviations – 1÷2 pixels in size – is possible between mineral phases of mineral map and large-area SEM images. To handle this minor mismatch the binary masks were morphologically eroded. The prepared binary masks were applied to the pre-registered SEM images, texture information was extracted from mineral phases of SEM data and analyzed. These data may be used in a texture-based segmentation method that allows identification of mineral phases and pseudo-phases in the areas of SEM images that are not covered with the mineral map.

Acquisition of FIB-SEM data

Zones of interest for FIB-SEM study were determined with the use of automated mineralogy and SEM data. The zones were analyzed for technical possibility of accessing them with FIB-SEM instruments. In a DualBeam system, the electron and ion beam columns intersect at a 52° angle near the sample surface, allowing immediate, high-resolution SEM imaging of the FIB-milled surface. With such an angle, some parts of the sample intersect with the line of view of SEM detectors — this limits the area of rock surface that can be accessed with FIB-SEM without cutting the sample. Some zones were physically too small for the analysis or are altered with artificial fractures or artefacts. As the result of the selection process, several suitable zones for FIB-SEM operations were identified. The most representative zone was selected with consideration of other elements attributed to zone's boundary, such as fractures along the interface of the mineral phase and rock matrix.

Acquisition of 3D FIB-SEM models were made with FEI Versa 3D DualBeam analytical system in the special way, to include the volume of a mineral grain/inclusion, the rock matrix, and the interface between the grain and the matrix into the same volume of the model. Scanning resolution for FIB-SEM models was 4÷6 nm/pixel, slice thickness was 25 nm. There were 500÷600 slices collected for each model, which made up for 15×15×15 μm physical size of the studied sample volume.

FIB-SEM data were processed with FEI PerGeos software. Original slices were filtered using Fast Fourier Transform to remove periodical artifacts in vertical and horizontal direction; individual slices were aligned with each other and the resulting stack was cropped to the volume that intersects all the slices; the non-local means smoothing and unsharp masking filters were applied to the dataset to remove high-frequency noise and increase edge contrast; the filtered dataset was segmented into minerals and pore-space. The pore space model was used for further analysis.

Results

In the project on multi-scale study of Berezov formation rock, there were studied seven Ø3 mm micro-scale sub-plugs, which were representative samples of larger Ø30 mm rock samples. The discussed methodology was applied to these sub-plugs. To illustrate the results of the proposed approach, the results for one of the sub-plugs are further discussed. Eventually, for the primary half-plug of the presented rock sample, the following dataset was obtained:

- automated mineralogy data
    - raw data (SIP file, EDS spectra, device configuration files);
    - original false-color mineral tiles;
    - false-color mineral stitched map;

    - mineral recognition and classification uncertainty stitched map;
    - lookup table describing a correspondence between false colors and mineral names;
- large-area SEM data
    - raw data, including device configuration files;
    - original false-color CBS and SE tiles;
    - stitched large-area high-resolution CBS and SE images.
- FIB-SEM data
    - raw data, including device configuration files;
    - original false-color SE slices;
    - EDS maps for the first and the last slice in the stack.

The mineral map of the rock sample, acquired with automated mineralogy and petrography method, contained 69 mineral phases (Figure 5), including pure minerals, two-mineral mixtures (for example "Chlorite-Albite (75:25)"), voids (pores), Unclassified sites, and trace elements/minerals. The size of the mineral map was 4,158×2,250 pixels with resolution 976.8 nm/pixel.

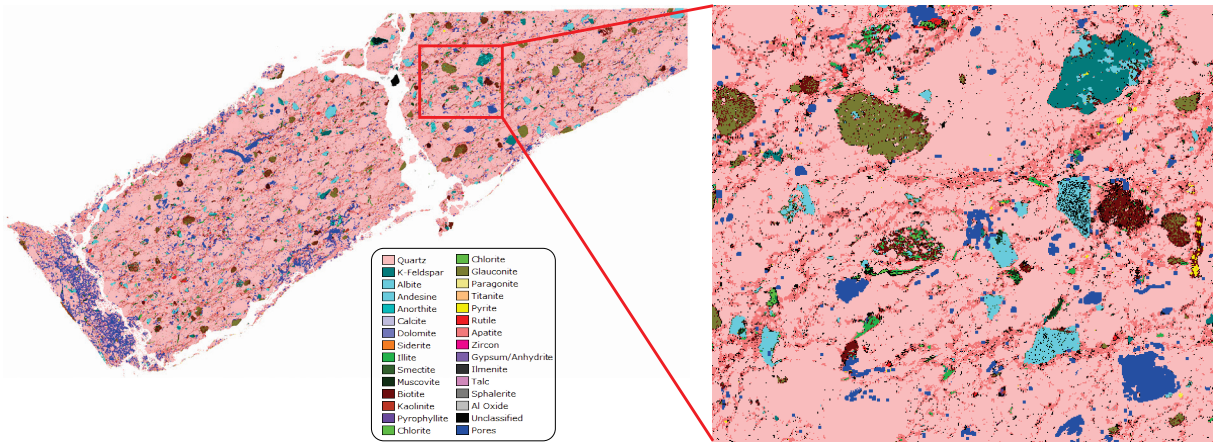

Figure 5: Original mineral map (left) and portion of the map zoomed in (right).

The results of SEM imaging were represented by two types of data — the original tiles, collected with SEM in CBS and SE modes, and the stitched large-area images. The original tiles were 8-bit Grayscale, they had the size of 6,144×4,096 pixels with resolution of 135 nm/pixel. The tiles were collected with overlaps, which were utilized by MAPS software for stitching the tiles into a large-area image. The large-area SEM image (Figure 6) had the size 22,813×91,624 pixels which corresponded, with respect to the overlapping areas, to the physical size of the imaged area of 3.08×12.3 mm.

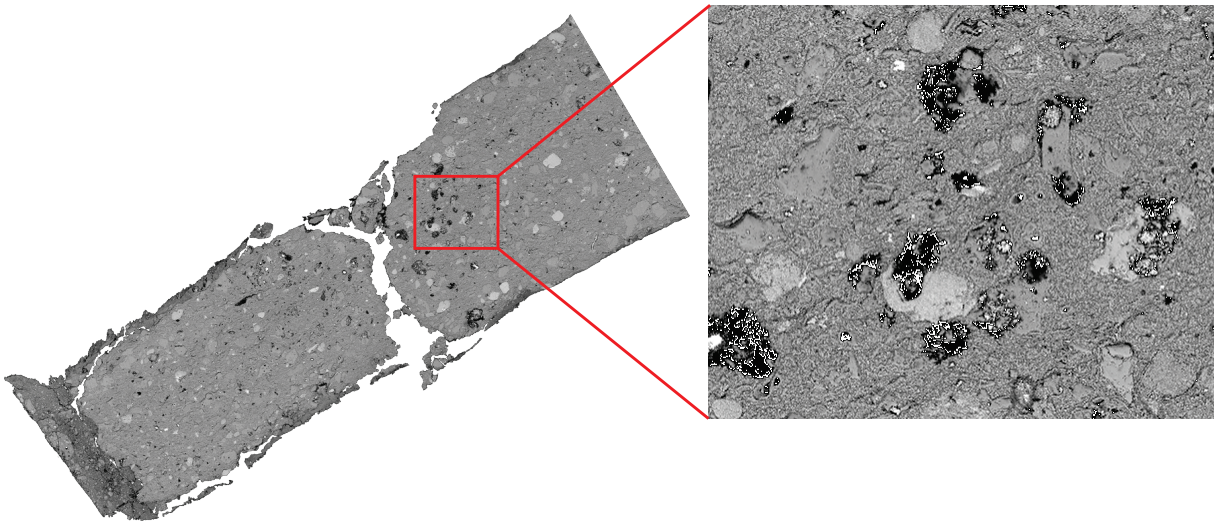

Figure 6: Original SEM CBS data (left) and its zoomed fragment (right).

SEM images were resampled to the resolution of mineral map images (976.8 nm/pixel) and registered to the mineral map. The result of registration is shown in Figure 7. The best registration results, with average misfit ~3 px, were achieved at *Mono* mode with *Similarity* transformation class.

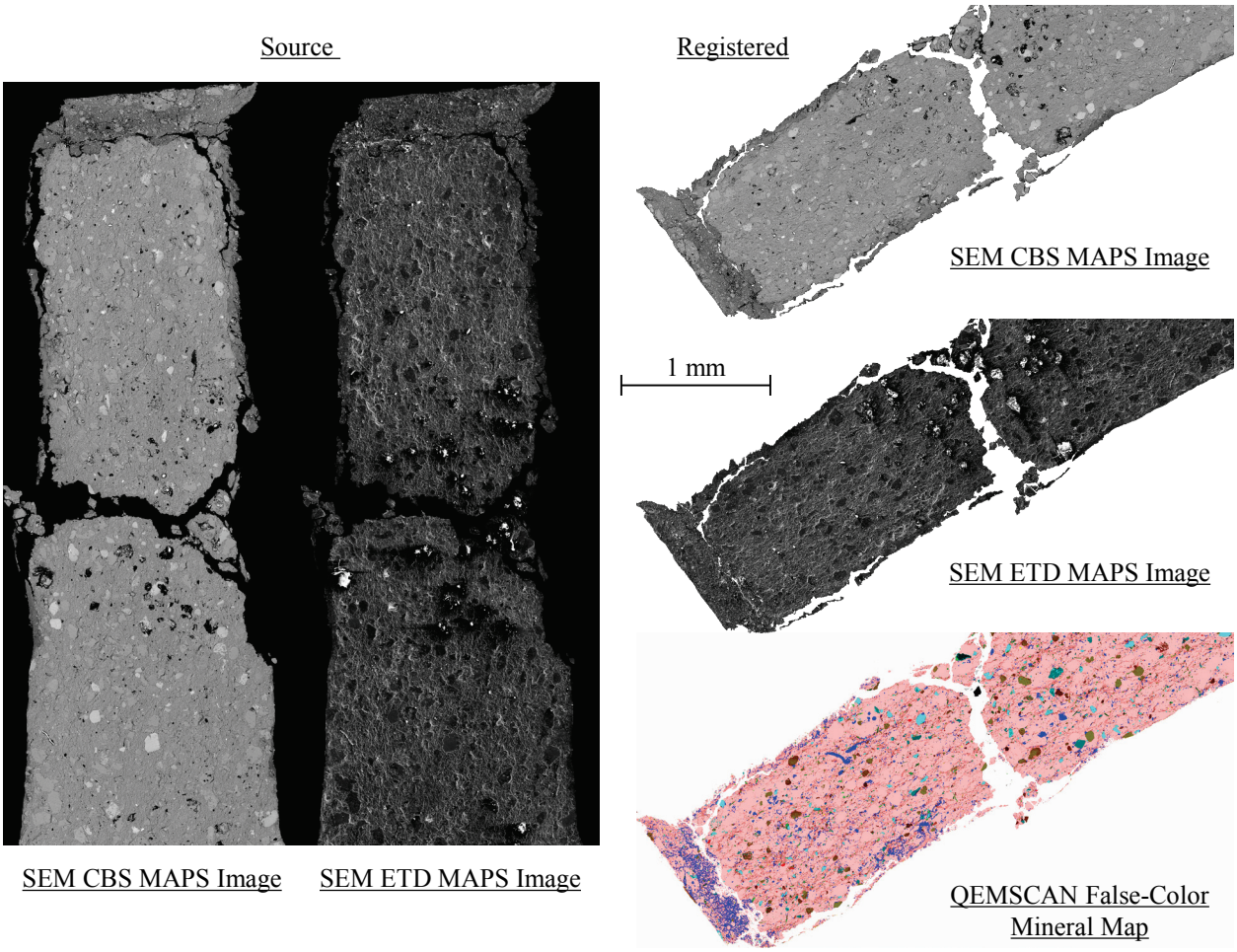

Figure 7: Input (left) and output (right) of image registration process.

At this step the registered images could be analyzed in a quantitative manner, in order to extract mineral composition and rock fabric parameters around any point at the rock sample surface (Figure 8). There are many ways and strategies of doing this.

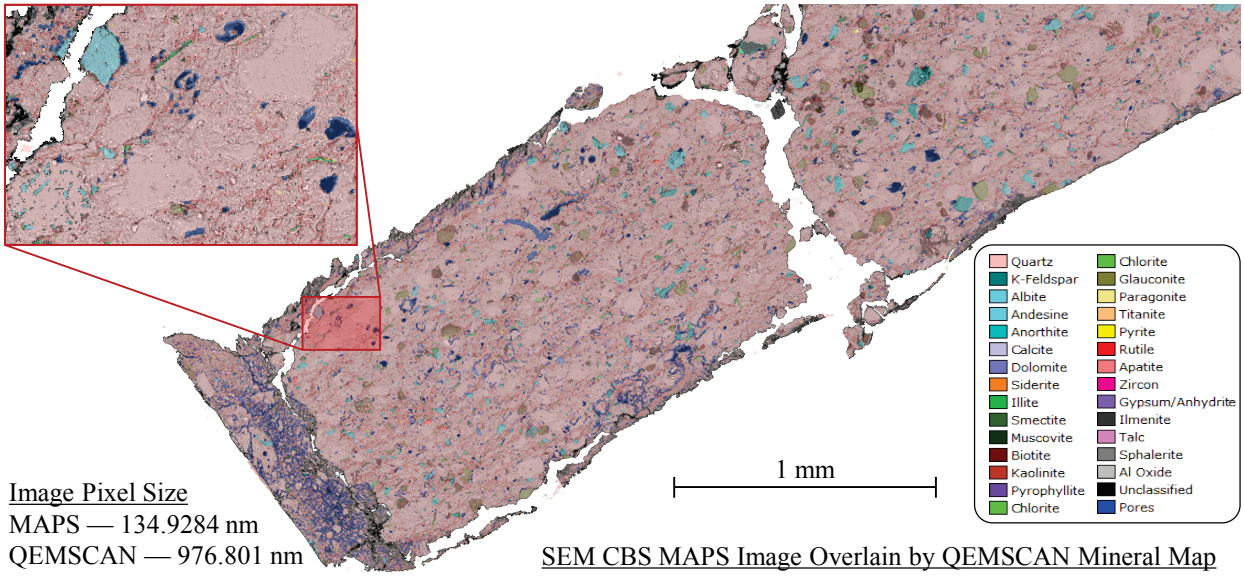

Figure 8: Concept of integrating mineral composition from automated mineralogy data at micron pixel size with microstructural information from FESEM at nanometer pixel size. A precise overlay of mineral masks on the nano-meter resolution microstructural images makes a fully integrated quantative analysis rock fabric and composition possible.

Post-processing of automated mineralogy data was accomplished in four steps (Figure 9). The "75:25" types of mineral phases were replaced with the "75" part — multiple variations of Quartz, Chlorite, Illite and other minerals were replaced by the major component, which visually removed single pixels and pixel clusters (Figure 9, top right). The number of indexed phases decreased from 69 to 32 — this included monominerals, voids, and unclassified pixels. Processing of Unclassified pixels ((Figure 9, bottom left) reduced the number of indexed phases to 31, but significantly improved smoothness of the mineral map by removing multiple single pixel occurrences of unclassified material. It should be mentioned that at some locations of the mineral map there were identified clusters of unclassified pixels, which were successfully processed by iterative application of the discussed method (Figure 10).

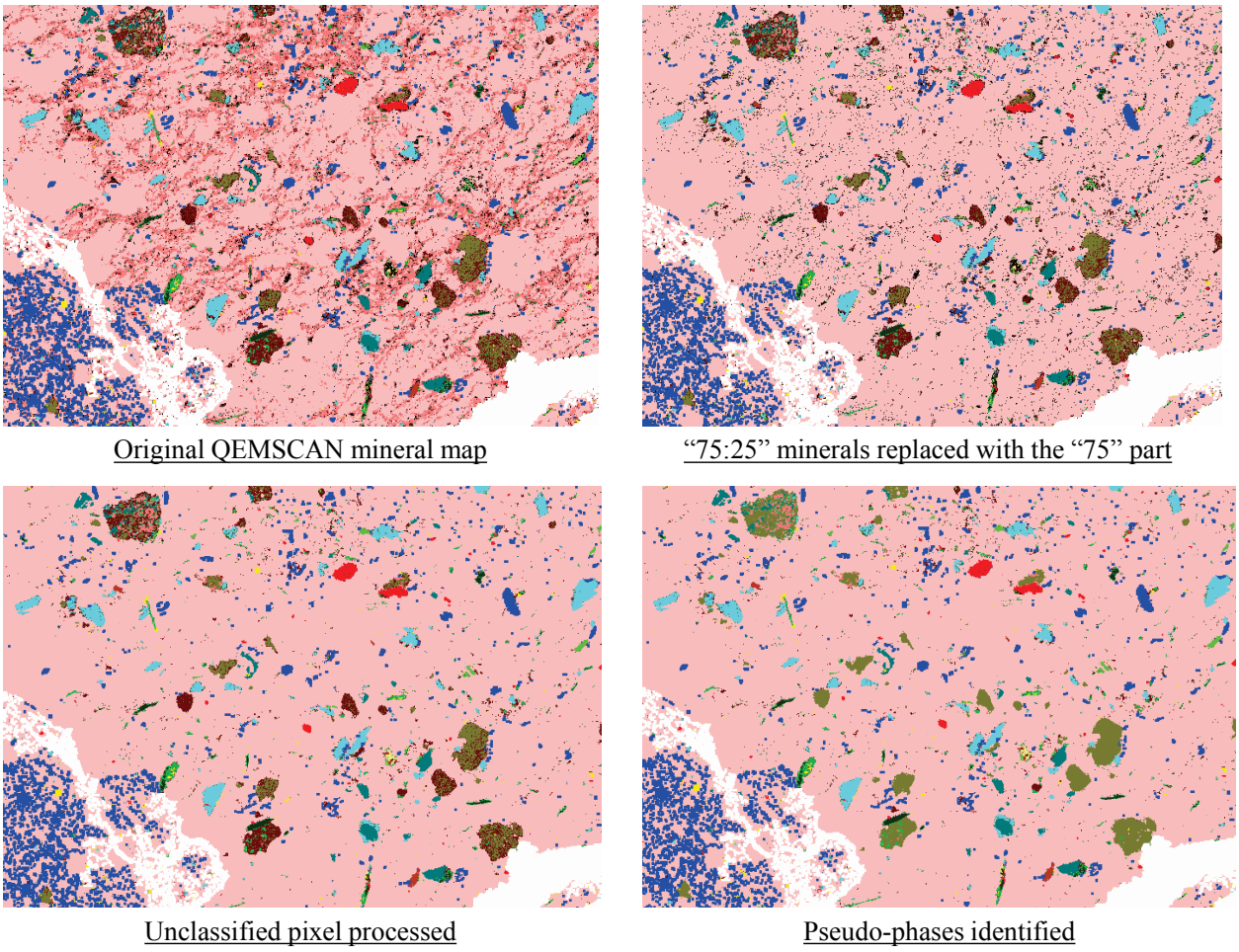

Figure 9: Processing steps of automated mineralogy data — a portion of the map is shown with zooming in to detailed representation of mineral phases; the shown are: the original map (top left), the map after processing of “75:25” mineral phases (top right), the map after processing of Unclassified pixels (bottom left), and the map after identification and filling in the pseudo-phases (bottom right) — results for Biotite-Glauconite pseudo-phase are shown in green color.

There were identified 6 pseudo-phases in the mineral map, a processing result for one of the pseudo-phases is shown in (Figure 9, bottom right). The pseudo-phases typically consist of 2 to 7 monominerals. The Biotite-Glauconite pseudo-phase, presented in Figure 9, consists of 2 minerals, but multiple single mineral inclusions within the pseudo-phase could be noticed. The type of the inclusions is not consistent — for some entries, the inclusions are presented by Illite, Albite, K-Feldspar, Apatite, and Chlorite, for other entries the inclusions are only presented by Apatite, and some pseudo-phases have no other inclusions. Such complex mixing of minerals within mineral grains requires additional geological interpretation and formulation of additional rules for pseudo-phase formulation.

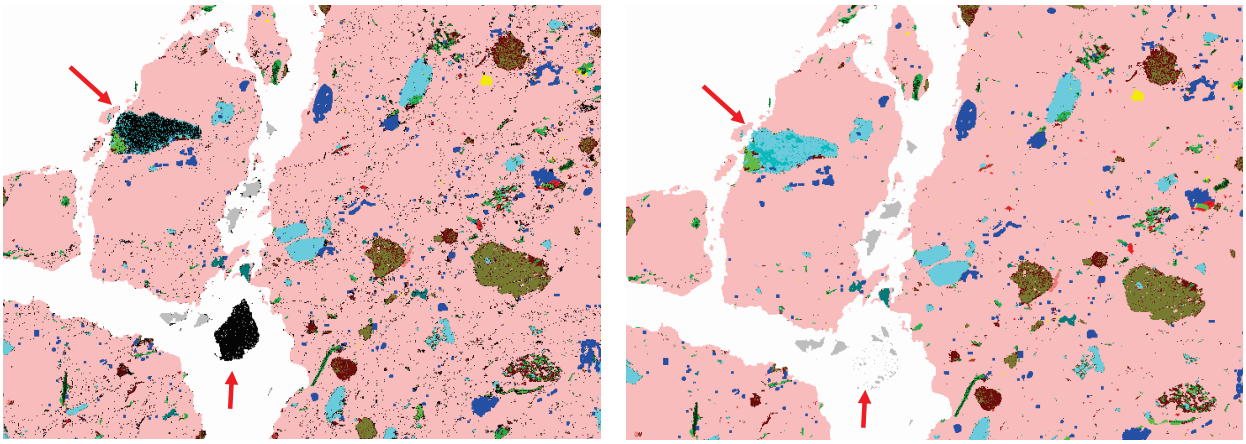

"75:25" minerals replaced with the "75" part

Unclassified pixel processed

Figure 10: Iterative processing of Unclassified pixels in automated mineralogy data allows handling large clusters of Unclassified pixels. The input image contained a few Unclassified clusters (left) shown with red arrows, the processed image has the Unclassified clusters replaced with the most frequently occuring mineral sampled in the close vicinity of the Unclassified pixel (right); the position of the Unclassified clusters is shown with red arrows.

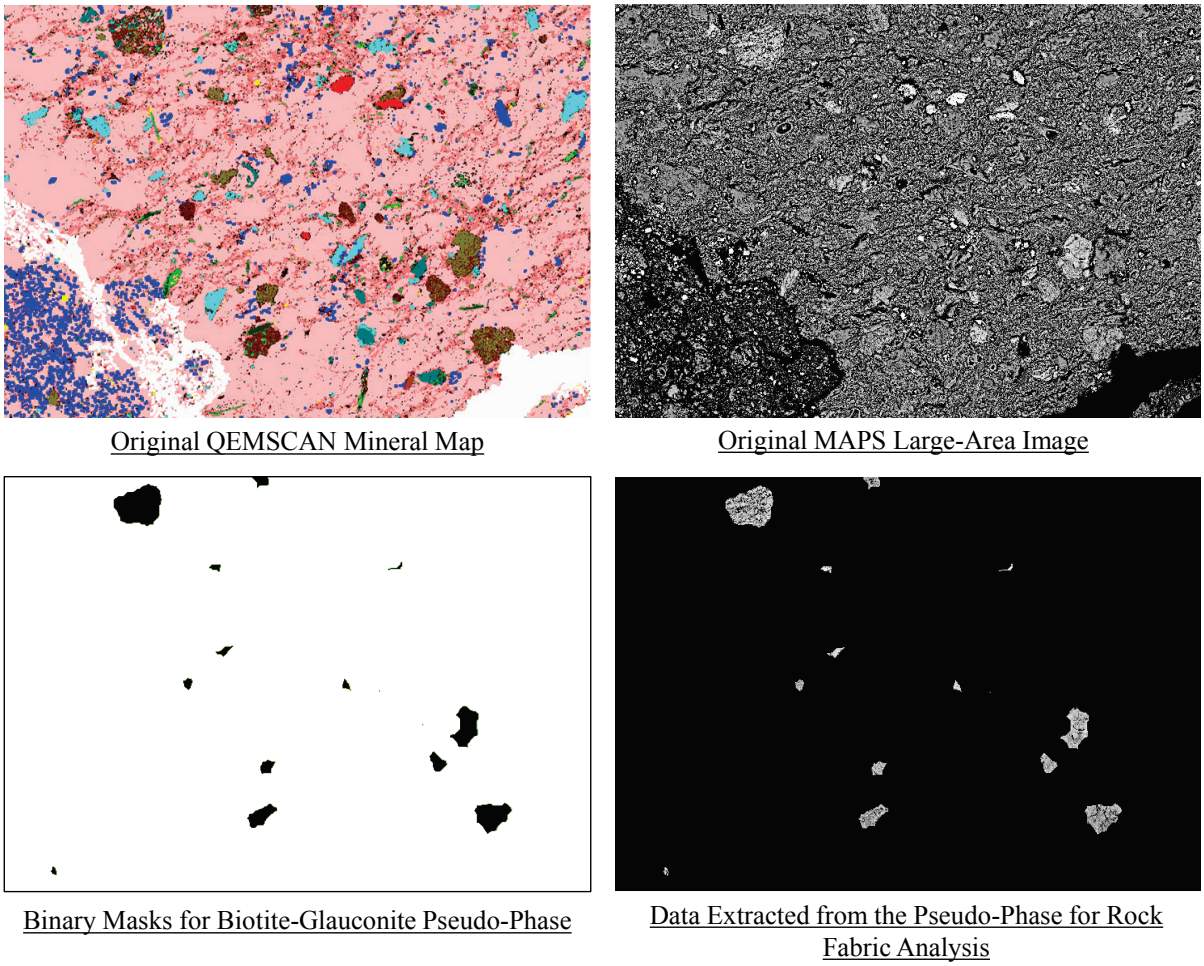

Original QEMSCAN Mineral Map

Original MAPS Large-Area Image

Binary Masks for Biotite-Glauconite Pseudo-Phase

Data Extracted from the Pseudo-Phase for Rock Fabric Analysis

Figure 11: Concept of integrating mineral composition from automated mineralogy at micron pixel size with microstructural information from SEM data at nanometer pixel size. A precise overlay of mineral masks on the nano-meter resolution microstructural images makes a fully integrated quantitative analysis of rock fabric and composition possible.

From all pseudo-phases and monomineral phases there were generated binary masks, which were additionally processed with morphological operators and applied to SEM images (Figure 11). Eventually, a comprehensive set of potential FIB-SEM site locations was established in the result of joint analysis of rock mineral composition and fabric maps for surface of each sample. For example, one site of the interest from mineral composition was defined at the location of a coupling of amorphous-crystalline siliceous-argillaceous mass (one of the major components of rock mineral matrix) to complex association of biotite and glauconite with inclusions of illite. From the standpoint of rock fabric is was described as a clay-like structural grain.

The shown case of Biotite-Glauconite pseudo-phase contains multiple types of texture at different locations of the same pseudo-phase. A mineral grain with inclusions of Illite was analyzed with the help of SEM data at the original resolution of 135 nm/pixel. Differently to other occurrences of the same pseudo-phase on sample's surface, the selected grain contained indications of possible nano-fractures (Figure 12, right). This grain was selected for analysis with FIB-SEM tool.

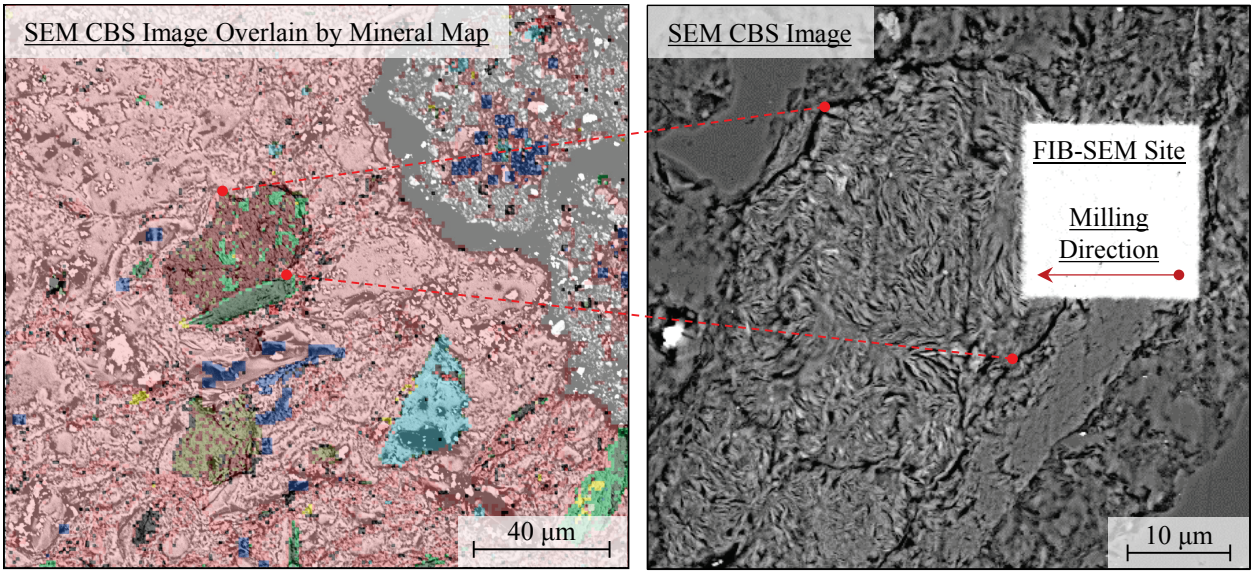

Figure 12: Example location of target FIB-SEM site based on rock fabric and mineral composition using Integration of large-area high-resolution SEM and automated mineralogy data (left) and selection of FIB milling direction (right).

A dataset acquired with FIB-SEM technique was used for building a 3D grayscale model of the target region (Figure 13). The model was segmented into voids and mineral matrix; the topology of pore space was analyzed for further applications in numerical modeling. In the result of pore connectivity analysis, it was found that the target 3D model contain a certain number of isolated (not interconnected) nanopores that demonstrate a potential for transformation of the main siliceous matrix into a permeable porous system, via a system of artificially induced intergranular nano- and micro-fractures.

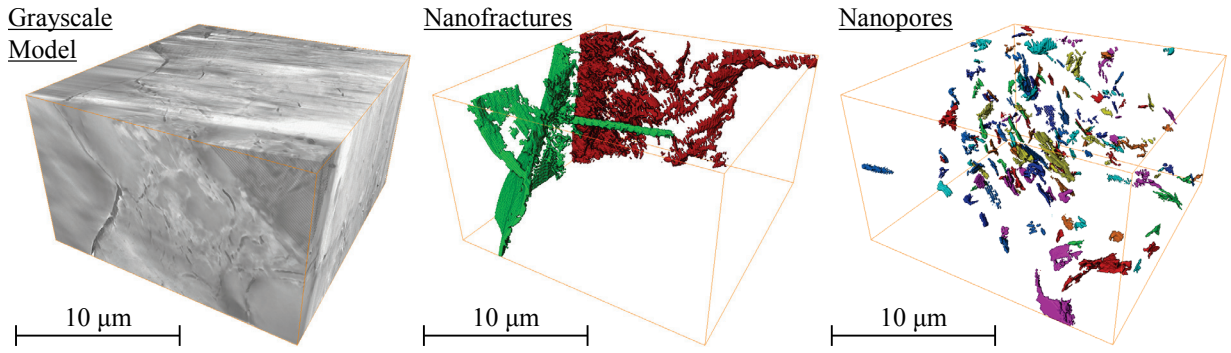

Figure 13: Target FIB-SEM model and results of its segmentation.

Results of this methodology are encouraging, 2÷200 nm/pixel point spacing SEM images have been registered and fused with 1 μm/pixel mineral map images; high-quality grain and void segmentation has been achieved. The integration of automated mineralogy and large-area high-resolution SEM data helped to separate mineral grains of certain categories from the rest of the minerals presented in SEM images, at the same time, the high resolution of SEM images helped to provide comprehensive analysis of rock fabric variation within the selected pseudo-phases and to select an individual mineral grain that contained important features for further analysis with 3D electron microscopy.

Conclusions

In the result of the applied research activity, an automated workflow for integrated analysis of large-area SEM images and automated mineralogy-based mineral maps was developed. The workflow is based on superposing nanometer-resolution large-area SEM images and micrometer-resolution mineralogy map images, supplemented with physics-based selection criteria for justified selection of candidate sites on rock surface for microstructural analysis at nano-scale.

The application of the workflow was demonstrated via analyzing a rock sample taken from one of Russian most promising tight gas formation, where pore space elements span from single nanometers to millimeters. The quantitative data obtained in the analysis allowed optimal spot selection for FIB-SEM operations. The workflow has and can be directly applied to a wide range of important problems including:

- full-featured analysis of rock heterogeneity in terms of mineral composition and fabric (*petrofabrics* or *petrotexture*) using advantages of high spatial resolution and mineral mapping capabilities of modern analytical tools;
- upscaling of physical-chemical properties of rock from the pore scale (nano- and micro-) to the scale of core sample and further to the scale of a borehole;
- optimization of quantity, extent and features of microstructural analysis operations (SEM, FIB-SEM, TEM, HIM) accounting for intrinsic rock heterogeneity of both fabric and mineral composition, as well as for particular project limitations: available sample area, budget, time, resources etc.;

Further work on data integration should be related to analysis of automated mineralogy data within particular pseudo-phases, including pattern recognition; and analysis of geological relations between mineral phases and pseudo-phases located in close vicinity of each other. Another application of the described methodology would be related to semi-automatic extraction and classification of rock fabric features.

Acknowledgments

NOVATEK, Moscow, Russia: for providing reservoir rock samples and fruitful discussions of the results.

Skolkovo Institute of Science and Technology, Moscow, Russia: Raisa Romushkevich for geological analysis of mineral associations using optical microscopy of thin sections and automated mineralogy false-color mineral maps.

Systems for Microscopy and Analysis (SMA), Moscow, Russia: Victor Zagvozdin and Alexander Grigoriev for providing automated mineralogy services and corresponding dataset.

Ignacio Arganda-Carreras for generous help in tuning bUnwarpJ plugin of ImageJ for large-scale registration of high-resolution images.

Abbreviations

BSE or BS — Back Scattered Electron Imaging Mode of SEM

CBS — Circular Backscatter Detector (utilized in SEM)

C-SEM — Cryo-Scanning Electron Microscopy

EDS — Energy-Dispersive X-Ray Spectroscopy

ETD — Everhart-Thornley Low Energy Secondary Electron Detector (utilized in SEM)

FE-SEM — Field-Emission Scanning Electron Microscopy

FIB-SEM — Focused Ion Beam Scanning Electron Microscopy

HIM — Helium Ion Microscopy

LUT — look-up table (for describing false-color 8-bit QEMSCAN mineral maps)

MAPS — technology for automatic acquisition of large SEM images and stitching it to a large high-resolution composite image, allowing to analyze large-extent high-resolution model of a sample

QEMSCAN — Quantitative Evaluation of Minerals by Scanning Electron Microscopy

RTI — Rock Texture Index

SE or SEI — Secondary Electron Mode Imaging Mode of SEM

SIFT — Scale Invariant Feature Transform

SIP — Species Identification Protocol (utilized in QEMSCAN)

TEM — Transmission Electron Microscopy

References

Agalakov, S. E. and Bakuev, O. V. 1992. New Objects of Hydrocarbon Prospecting in Over-Cenomanian Deposits of the Western Siberia. *Oil and Gas Geology* (11): 25–28.

Bondarev, V. L., Mirotvorsky, M. Y., Zvereva, V. B. *et al.* 2008a. Gas-Chemical Characteristics of Above-Senoman Deposits of Yamal Peninsula (Case Study at Bovanenkovo Gas-Condensate Deposit). *Geology, Geophisics and Development of Oil and Gas Deposits* (5): 22–34.

Bondarev, V. L., Mirotvorsky, M. Y., Zvereva, V. B. *et al.* 2008b. Unconventional Gas Deposits in the North of West Siberia. *Geology, Geophisics and Development of Oil and Gas Deposits* (10): 4–16.

Borodina, E. A. 2016. Berezovskaya Formation — New Approaches to Evaluation of Petroleum Potential Witnin the Western Siberia. Geomodel 2016. 18th Science and Applied Research Conference on Oil and Gas Geological Exploration and Development, Gelendzhik, Russia, September 12–15, 2016.

Bouw, S. S. and Lutgert, J. 2012. Shale Plays in The Netherlands. SPE/EAGE European Unconventional Resources Conference and Exhibition, Vienna, Austria, March 20–22, 2012. SPE-152644-MS. http://dx.doi.org/10.2118/152644-MS.

Butcher, A. R., Helms, T. A., Gottlieb, P. *et al.* 2000. Advances in the Quantification of Gold Deportment by QEMSCAN. Seventh Mill Operators' Conference, Kalgoorlie, Western Australia, October 12–14, 2000.

Fogden, A., Goergen, E., Olson, T. *et al.* 2015. Applications of Multi-Scale Imaging Techniques to Unconventional Reservoirs. SPE Asia Pacific Unconventional Resources Conference and Exhibition, Brisbane, Australia, 9–11 November 2015. SPE-176948-MS.

Goergen, E. T., Curtis, M. E., Jernigen, J. *et al.* 2014. Integrated Petrophysical Properties and Multi-Scaled SEM Microstructural Characterization. Unconventional Resources Technology Conference, Denver, Colorado, USA, August 25–27, 2014. URTEC-1922739-MS. http://dx.doi.org/10.15530/URTEC-2014-1922739.

Goldstein, J., Newbury, D. E., Joy, D. C. *et al.* 2003. *Scanning Electron Microscopy and X-ray Microanalysis*, Third·edition: Springer.

Hussain, M., Minhas, N.-U.-R., Saad, B. *et al.* 2017. Rock Texture Characterization from Automated Petrographic Analysis. SPE Middle East Oil & Gas Show and Conference, Manama, Kingdom of Bahrain, 6–9 March 2017. SPE-184007-MS.

Hussain, M., Minhas, N., Agrawal, G. *et al.* 2016. Could Diagenesis in Carbonate Source Rock Predefine Its Fracturing Behavior? Unconventional Resources Technology Conference (URTeC 2016), San Antonio, Texas, USA, August 1–3, 2016. URTEC-2454614-MS. http://dx.doi.org/10.15530/URTEC-2016-2454614.

Lattanzi, D. A., Salazar, L., Jaime, P. I. *et al.* 2014. Registration and Fusion of Backscattered Electron Images and Energy Dispersive Spectroscopy Images on Siliciclastic Rock Samples for Petrophysical Calculations. SPE Latin American and Caribbean Petroleum Engineering Conference, Maracaibo, Venezuela, May 21–23, 2014 SPE-169332-MS. http://dx.doi.org/10.2118/169332-MS.

Liao, G., Sun, L., Liu, G. *et al.* 2015. Numerical Simulation of Petrophysical Properties with Multi-Scale Digital Rock Techniques of Tight Oil Reservoir. SEG New Orleans Annual Meeting, New Orleans, Louisiana, USA. http://dx.doi.org/10.1190/segam2015-5855520.1.

Madi, J. A. and Belhadj, E. M. 2015. Unconventional Shale Play in Oman: Preliminary Assessment of the Shale Oil / Shale Gas Potential of the Silurian Hot Shale of the Southern Rub al-Khali Basin. SPE Middle East Unconventional Resources Conference and Exhibition, Muscat, Oman, 26–28 January 2015. SPE-172966-MS.

Mathieu, J.-P., Leduc, J.-P., Pelletier, J. *et al.* 2016. Assessment of Rock Types Properties in a South American Unconventional Shale Play. Unconventional Resources Technology Conference (URTeC 2016), San Antonio, Texas, USA, August 1–3, 2016. URTEC-2460086-MS. http://dx.doi.org/10.15530/URTEC-2016-2460086.

Minhas, N.-U.-R., Saad, B., Hussain, M. *et al.* 2016. Big Data Hiding in Small Rocks: Case Study of Advanced Microscopy and Image Processing to Aid Upstream Asset Development. SPE Kingdom of Saudi Arabia Annual Technical Symposium and Exhibition, Dammam, Saudi Arabia, 25–28 April 2016. SPE-182821-MS.

Owen, M. 2016. "Announcing a New Technique for SEM Super-Resolution Mineral Analysis ", accessed Tuesday, 24 May 2016. http://automatedmineralogy.blogspot.com.es/2016/05/announcing-new-technique-for-sem-super.html.

Plumb, R. A. 1994. Influence of Composition and Texture on the Failure Properties of Clastic Rocks. Rock Mechanics in Petroleum Engineering, Delft, Netherlands, August 29–31, 1994. SPE-28022-MS. http://dx.doi.org/10.2118/28022-MS.

Plumb, R. A., Herron, S. L. and Olsen, M. P. 1992. Composition and Texture on Compressive Strength Variations in the Travis Peak Formation. SPE Annual Technical Conference and Exhibition, Washington, D.C., USA, October 4–7, 1992. SPE-24758-MS. http://dx.doi.org/10.2118/24758-MS.

Sander, B. 1930. *Gefügekunde der Gesteine*. Berlin, Vienna: Julius Springer.

Schembre-McCabe, J., Salazar-Tio, R. and Kamath, J. 2012. Two Examples of Adding Value Through Digital Rock Technology. International Symposium of the Society of Core Analysts, Aberdeen, Scotland, UK, 27–30 August 2012. SCA2012-18.

Sølling, T. I., Mogensen, K. and Gerwig, T. 2014. On Diverse Applications of QEMSCAN in the Oil and Gas Industry (and Beyond). International Symposium of the Society of Core Analysts, Avignon, France, September 8–11, 2014. SCA2014-040.